Ganesh Kumar *et al. International Journal of Mechanical and Materials Engineering* (2017) 12:18
DOI 10.1186/s40712-017-0083-5

International Journal of Mechanical and Materials Engineering

ORIGINAL PAPER Open Access

Effect of nonlinear thermal radiation on double-diffusive mixed convection boundary layer flow of viscoelastic nanofluid over a stretching sheet

K. Ganesh Kumar[1], B. J. Gireesha[1], S. Manjunatha[2*] and N. G. Rudraswamy[1]

Abstract

Background: The present exploration deliberates the effect of nonlinear thermal radiation on double diffusive free convective boundary layer flow of a viscoelastic nanofluid over a stretching sheet. Fluid is assumed to be electrically conducting in the presence of applied magnetic field. In this model, the Brownian motion and thermophoresis are classified as the main mechanisms which are responsible for the enhancement of convection features of the nanofluid. Entire different concept of nonlinear thermal radiation is utilized in the heat transfer process.

Methods: Appropriate similarity transformations reduce the nonlinear partial differential system to ordinary differential system which is then solved numerically by using the Runge–Kutta–Fehlberg method with the help of shooting technique. Validation of the current method is proved by having compared with the preexisting results with limiting solution.

Results: The effect of pertinent parameters on the velocity, temperature, solute concentration and nano particles concentration profiles are depicted graphically with some relevant discussion and tabulated result.

Conclusions: It is found that the effect of nanoparticle volume fraction and nonlinear thermal radiation stabilizes the thermal boundary layer growth. Also it was found that as the Brownian motion parameter increases, the local Nusselt number decreases, while the local friction factor coefficient and local Sherwood number increase.

Keywords: Double diffusion, Mixed convection, Nanofluid, Viscoelastic fluid, Nonlinear thermal radiation

Background

In the modern day, a great deal of interest has been created on heat and mass transfer of the boundary layer flow over a stretching sheet, in view of its numerous applications in various fields such as polymer processing industry in manufacturing processes. Sakiadis (1961a; Sakiadis, 1961b) first studied the boundary layer problem assuming velocity of a bounding surface as constant. Crane (1970) computed an exact similarity solution for the boundary layer flow of a Newtonian fluid toward an elastic sheet which is stretched with velocity proportional to the distance from the origin. It is noteworthy to mention that both of these studies are regarding Newtonian fluid. Subsequently, the pioneering works of Sakiadis and Crane have been extended by including various effects such as suction/injection, porosity, magnetic field, variable material properties, thermal radiation, heat source/sink, and slip boundary, for either a Newtonian or non-Newtonian fluids. In recent years, researches on boundary layer flow and heat transfer in nanofluids have received amplified devotion due to their growing importance in numerous industrial and biomedical applications. Nanofluid is dilute suspension of nanoparticles with at least one of their principal dimensions smaller than 100 nm and the base fluid. Nanofluids are very stable and free from extra issues of sedimentation, erosion, additional pressure drops, and rheological characteristics. This is due to the tiny size and the low-volume fraction of nanoelements. Thus, nanofluids have principal advantage about enhancement in thermal conductivity and the convective heat transfer coefficient when compared with the customary base fluids which comprise water, oil, and ethylene glycol. The nanomaterials are more operative in terms of heat

* Correspondence: manjubhushana@gmail.com
[2]Faculty of Engineering, Department of Engineering Mathematics, Christ University, Mysore Road, Bengaluru 560074, India
Full list of author information is available at the end of the article

exchange performance in micro/nanoelectro mechanical devices, for growing demands of modern technology, including power station, chemical production, and microelectronics. Especially, the magneto nanofluids are significant in applications like optical modulators, magneto-optical wavelength filters, tunable optical fiber filters, and optical switches. Choi (1995) was first to use the term nanofluids to refer to the fluid with suspended nanoparticles. Thermophysical properties of nanofluids such as thermal conductivity, diffusivity, and viscosity have been studied by Kang et al. (2006). The theoretical/experimental investigations on nanofluid flow and heat transfer were conducted by Rudyak et al. (2010), Wang et al. (1999), Eastman et al. (2001), and Rudraswamy et al. (2016; 2015) initiated an incompressible nanofluid over an impermeable stretching sheet and considered the uniform magnetic field. To make such investigations, the following studies are quite useful (Kai-Long Hsiao (2016; Hsiao 2014; Hsiao 2017a; Hsiao 2017b; Hsiao 2017b) Buongiorno (2006), Khan and Pop (2010), and Kuznetsov and Nield (2010)). They concluded that the nanofluids possess the novel property of enhanced thermal conductivity of the working fluids.

Researchers are paying their attention to investigate the properties of non-Newtonian fluids because of their numerous technological applications, including manufacturing of plastic sheets, performance of lubricants, and movement of biological fluids. Nadeem et al. (2014) initiated the boundary-layer flow and heat transfer of a Maxwell fluid past a stretching sheet. Shehzad et al. (2015) have observed the influence of nanoparticles in MHD flow of Jeffrey fluid over a stretched surface, and they considered the thermal and nanoparticle concentration convective boundary conditions. Khan and Gorla (2011) studied heat and mass transfer in non-Newtonian nanofluids over a stretching surface with prescribed wall temperature and surface nanoparticle concentration. Recently, Rizwan et al. (2014), Ganesh et al. (2017), and Rudraswamy et al. (2017) also discussed the nanofluid in the presence of Newtonian heating and viscous dissipation over a stretching sheet (Fig. 1).

During the past four decades, the investigators have devoted to the double-diffusive phenomena because of their various applications in chemical engineering, solid-state physics, oceanography, geophysics, liquid gas storage, production of pure medication, oceanography, high-quality crystal production, solidification of molten alloys, and geothermally heated lakes and magmas, etc. Khan and Aziz (2011) analyzed the double-diffusive natural convective boundary layer flow in a porous medium saturated with a nanofluid over a vertical plate with prescribed surface heat, solute, and nanoparticle fluxes. Nield and Kuznetsov (2011) presented the double-diffusive nanofluid convection in a porous medium using analytical method. Numerous models and methods have been proposed by

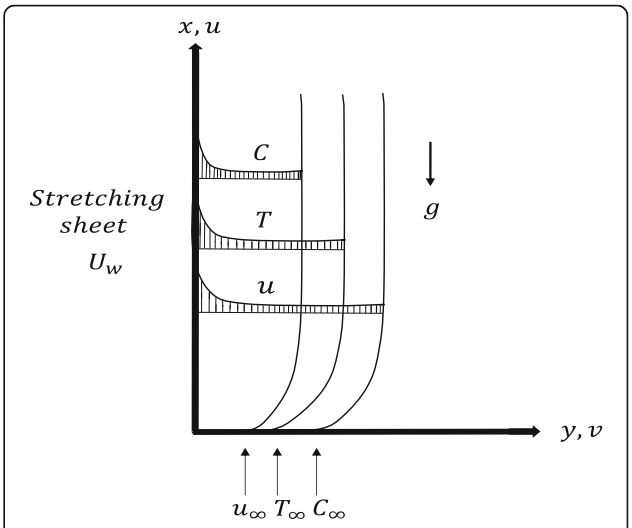

Fig. 1 Geometry of the problem

many researchers and academicians to advance their studies relating to problems involving various parameters. To make such investigations, the following studies are quite useful (Sharma et al. (2012), Hayat et al. (2014), Beg et al. (2014), Goyal and Bhargava (2014), Gaikwad et al. (2007), Wang (1989), and Gorla and Sidawi (1994)).

Motivated by the aforementioned researchers, we have considered the level of species concentration is moderately high so that the thermal diffusion (Soret) and diffusion-thermo (Dufour) effects cannot be neglected. In view of the above discussion, the necessity of Soret and Dufour effects and inclusion of nonlinear thermal radiation in the heat transfer and first-order chemical reaction not only enrich the present analysis but also complement the earlier studies. The inclusion of these phenomena gives rise to additional parameters such as viscoelastic parameter, Brownian motion parameter, thermophoresis parameter, modified Dufour parameter, regular double-diffusive buoyancy ratio, nanofluid buoyancy ratio, mixed convection parameter, radiation parameter, Dufour Lewis number, nanofluid Lewis number, and regular Lewis number. Thus, inclusion of additional parameters contributes to the complexity of the mathematical model representing the flow, heat, and mass transfer phenomena. To the best of author's acquaintance, no work has been so far reported considering above phenomenal together.

Mathematical formulation

Consider a steady two-dimensional laminar flow of an incompressible and electrically conducting viscoelastic nanofluid over a stretching surface. The flow models for elastic-viscous and double-diffusive are considered. The Brownian motion and thermophoresis are taken into consideration. It is also assumed that in its plane, the surface of the sheet is stretched with the velocity $u_w = ax$

Table 1 Comparison of the result for Nusselt number $-\theta'(0)$ when Nd = Le = Ld = $\alpha = \lambda = 0$, Bi = 1 , $R = 1$, $\theta_w = 1$, $M = 1.5$, Nc = 0.1, Ln = 0, Nb = Nt $\rightarrow \infty$

Pr	Khan and Pop (2010)	Wang (1989)	Gorla and Sidawi (1994)	Goyal, and Bhargava (2014)	Present result (RKF-45 method)
0.7	0.4539	0.4539	0.5349	0.4539	0.46257
2	0.9113	0.9114	0.9114	0.9113	0.91135
7	1.8954	1.8954	1.8905	1.8954	1.89539
20	3.3539	3.3539	3.3539	3.3539	3.35387
70	6.4621	6.4622	6.4622	6.4621	6.46209

(where $a > 0$ is the constant acceleration parameter). The x-axis is taken vertically upwards, and flow is confind in the region at $y = 0$. T_w, C_w, and N_w denote the constant values of the temperature, solutal concentration, and the nanoparticle concentration at the boundary and at the large distance from the sheet ($y \rightarrow \infty$), the temperature, solutal concentration, and the nanoparticle concentration are represented by T_∞, C_∞, and N_∞, respectively. It is worth mentioning that $T_w > T_\infty$, $C_w > C_\infty$, and $N_w > N_\infty$ as a results of these conditions, the momentum, thermal, solutal, and nanoparticle concentration boundary layers are formed near the solid surface. The sheet is saturated in a medium which is saturated by a binary fluid with dissolved solutal and containing nanoparticles in suspension. The fluid phase and nanoparticles both are assumed to be in thermal equilibrium state. The thermo physical properties of the nanofluid are assumed to be constant. Under the usual boundary layer approximation, the five governing equations were derived by Buongiorno (2006), Khan and Pop (2010), and Kuznetsov and Nield (2010), which represent equations of conservation of mass, momentum, thermal energy, solute, and nanoparticles.

$$\frac{\partial u}{\partial x} + \frac{\partial v}{\partial y} = 0, \tag{1}$$

$$u\frac{\partial u}{\partial x} + v\frac{\partial u}{\partial y} = v\frac{\partial^2 u}{\partial y^2} + \frac{\alpha}{\rho}\left[\frac{\partial u}{\partial x}\frac{\partial^2 u}{\partial y^2} + u\frac{\partial^3 u}{\partial x \partial y^2} + \frac{\partial u}{\partial y}\frac{\partial^2 u}{\partial y^2} + v\frac{\partial^3 u}{\partial y^3}\right] + \begin{bmatrix} -g\left(\rho_p - \rho_f\right)(N - N_\infty) + \\ (1 - N_\infty)\rho_f\left[g\beta_T(T - T_\infty) + g\beta_c(C - C_\infty)\right] \end{bmatrix} - \frac{\sigma B_0^2}{\rho}u, \tag{2}$$

$$u\frac{\partial T}{\partial x} + v\frac{\partial T}{\partial y} = \alpha_m\frac{\partial^2 T}{\partial y^2} + \tau\left[D_B\frac{\partial N}{\partial y}\frac{\partial T}{\partial y} + \frac{D_T}{T_\infty}\left(\frac{\partial T}{\partial y}\right)^2\right] + D_{TC}\frac{\partial^2 C}{\partial y^2} + \frac{\partial q_r}{\partial y}, \tag{3}$$

$$u\frac{\partial C}{\partial x} + v\frac{\partial C}{\partial y} = D_S\frac{\partial^2 C}{\partial y^2} + D_{CT}\frac{\partial^2 T}{\partial y^2}, \tag{4}$$

$$u\frac{\partial N}{\partial x} + v\frac{\partial N}{\partial y} = D_B\frac{\partial^2 N}{\partial y^2} + \frac{D_T}{T_\infty}\frac{\partial^2 T}{\partial y^2}. \tag{5}$$

The boundary conditions to the problem are given as follows:

$$u = u_w, \quad v = 0, \quad -k\frac{\partial T}{\partial y} = h_f\left(T_f - T\right), C = C_w, \quad N = N_w \text{at} y = 0,$$

$$u = v = 0, \quad T \rightarrow T_\infty, \quad C \rightarrow C_\infty, \quad N \rightarrow N_\infty \text{as} y \rightarrow \infty, \tag{6}$$

where u and v are the components of velocity along the x and y directions, ρ_f is the density of base fluid, ρ_p is the nanoparticle density, μ is the absolute viscosity of the base fluid, v is the kinematic viscosity of the base fluid, σ is the electrical conductivity of the base fluid, α is the material fluid parameter, T is the fluid temperature,

Table 2 Comparison of the results for the Nusselt number ($-\theta'(0)$) when Ln = Pr = 10 and Nd = Le = Ld = $\alpha = \lambda = 0$, Bi = 1 , $M = 1.5$, Nc = 0.1 , $R = 1$, $\theta_w = 1$

Nt	$-\theta'(0)$											
	Nb = 0.1			Nb = 0.2			Nb = 0.3			Nb = 0.4		
	Khan and Pop	Goyal and Bhargava	Present result	Khan and Pop	Goyal and Bhargava	Present result	Khan and Pop	Goyal and Bhargava	Present result	Khan and Pop	Goyal and Bhargava	Present result
0.1	0.9524	0.95244	0.95234	0.5056	0.50561	0.50556	0.2522	0.25218	0.25215	0.1194	0.11940	0.11940
0.2	0.6932	0.69318	0.69317	0.3654	0.36536	0.36536	0.1816	0.18159	0.18159	0.0859	0.08588	0.08590
0.3	0.5201	0.52025	0.52009	0.2731	0.27313	0.27311	0.1355	0.13564	0.13552	0.0641	0.06424	0.06408
0.4	0.4026	0.40260	0.40261	0.2110	0.21100	0.21100	0.1046	0.10461	0.10462	0.0495	0.04962	0.04947
0.5	0.3211	0.32105	0.32109	0.1681	0.16811	0.16810	0.0833	0.08342	0.08331	0.0394	0.03932	0.03939

Table 3 Comparison of the results for the nanoparticle Sherwood number ($-\varphi'(0)$) when Ln = Pr = 10 and Nd = Le = Ld = $\alpha = \lambda = 0$, Bi = 1 , $M = 1.5$, Nc = 0.1 , $R = 1$, $\theta_w = 1$

Nt	$-\varphi'(0)$											
	Nb = 0.1			Nb = 0.2			Nb = 0.3			Nb = 0.4		
	Khan and Pop	Goyal and Bhargava	Present result	Khan and Pop	Goyal and Bhargava	Present result	Khan and Pop	Goyal and Bhargava	Present result	Khan and Pop	Goyal and Bhargava	Present result
0.1	2.1294	2.12949	2.1290	2.3819	2.38186	2.3816	2.4100	2.41009	2.4098	2.3997	2.39970	*2.3994*
0.2	2.2740	2.27401	2.2735	2.5152	2.51537	2.5148	2.5150	2.51501	2.5147	2.4807	2.48066	*2.4804*
0.3	2.5286	2.52855	2.5284	2.6555	2.65550	2.6550	2.6088	2.60876	2.6084	2.5486	2.54848	2.5483
0.4	2.7952	2.79520	2.7949	2.7818	2.78181	2.7812	2.6876	2.68758	2.6871	2.6038	2.60380	2.6034
0.5	3.0351	3.03511	3.0334	2.8883	2.88830	2.8876	2.7519	2.75190	2.7513	2.6483	2.64831	2.6478

C is the solutal concentration, N is the nanoparticle volume fraction, $\alpha_m = \frac{k}{(\rho_C)_f}$ is the thermal diffusivity of the fluid, $\tau = \frac{(\rho c)_p}{(\rho c)_f}$ is the ratio of effective heat capacity of nanoparticle material to heat capacity of fluid, T_f is the hot fluid at temperature, D_{TC} and D_{CT} are the Dufour and Soret type diffusivity, D_S is the solutal diffusivity, D_B and D_T are the Brownian diffusion coefficient and thermophoresis diffusion coefficient, β_C is the volumetric solutal expansion coefficient of the fluid, β_T the is volumetric thermal expansion coefficient of the fluid, h_f is the heat transfer coefficient and g and k are the acceleration due to gravity and thermal conductivity of the fluid, respectively.

The Rosseland diffusion approximation for radiation heat flux q_r is given by

$$q_r = -\frac{16\sigma^*}{3k^*}T^3\frac{\partial T}{\partial y}, \tag{7}$$

where σ^* and k^* are the Stefan–Boltzmann constant and the mean absorption coefficient, respectively.

In view of Eq. (7), Eq. (3) reduces to

$$u\frac{\partial T}{\partial x} + v\frac{\partial T}{\partial y} = \frac{\partial}{\partial y}\left[\left(\alpha + \frac{16\sigma^* T^3}{3k^*}\right)\frac{\partial T}{\partial y}\right] + \tau\left[D_B\frac{\partial T}{\partial y}\frac{\partial C}{\partial y} + \frac{D_T}{T_\infty}\left(\frac{\partial T}{\partial y}\right)^2\right] + D_{TC}\frac{\partial^2 C}{\partial y^2}. \tag{8}$$

Yang et al. [38] have shown that a similarity relation is not possible for flows in stably stratified media. Similarity transformation is possible only for the case of temperature decreasing with height, which is physically unstable. Such is the present case, and hence, Eqs. (2) to (5) subjected to boundary conditions (6) admit self-similar solution in terms of the similarity function $f(\eta)$, $\theta(\eta)$, $\gamma(\eta)$, and $\phi(\eta)$ and the similarity variable η which is defined as follows:

$$u = axf'(\eta), v = -\sqrt{av}f(\eta), \eta = \sqrt{\frac{a}{\nu}}y,$$

$$T = T_\infty(1 + (\theta_w - 1)\theta), \gamma(\eta) = \frac{C - C_\infty}{C_w - C_\infty}, \phi(\eta) = \frac{N - N_\infty}{N_w - N_\infty}, \tag{9}$$

where $\theta_w = \frac{T_f}{T_\infty}$, $\theta_w > 1$ being the temperature ratio parameter.

Substituting the expressions in Eq. (9) into Eqs. (2)–(5), we obtain the following transformed similarity equations:

$$f''' + ff'' - f'^2 - \alpha\left(f''^2 - 2f'f''' + ff''''\right) + \lambda(\theta + Nc\,\gamma - Nr\phi) - Mf' = 0, \tag{10}$$

$$\left(1 + R\frac{d}{d\eta}(1 + (1 + \theta_w)\theta)^3\right)\theta''(\eta) + \Pr\left(f\theta' + Nb\theta' f' + Nt\theta'^2 + Nd\gamma''\right) = 0, \tag{11}$$

$$\gamma'' + Lef'\gamma' + Ld\theta'' = 0, \tag{12}$$

$$\phi'' + Lnf\phi' + \frac{Nt}{Nb}\theta'' = 0. \tag{13}$$

The transformed boundary conditions are

$$f(0) = 0,\ f'(0) = 1,\quad \theta'(0) = -Bi(1 - \theta(0)),\quad \gamma(0) = 1,\quad \phi(0) = 1 \text{ at } \eta = 0$$
$$f'(\infty) \to 0,\quad \theta(\infty) \to 0,\quad \gamma(\infty) \to 0,\quad \phi(\infty) \to 0 \text{ at } \eta \to \infty \tag{14}$$

where $\alpha = \frac{\alpha_1 a}{\mu}$ is the viscoelastic parameter, $Nb = \frac{(\rho C)_p D_B (N_w - N_\infty)}{(\rho C)_f \nu}$ is the Brownian motion parameter, $Nt = \frac{(\rho C)_p D_T (T_f - T_\infty)}{(\rho C)_f T_\infty \nu}$ is the thermophoresis parameter, $Nd = \frac{D_{TC}(T_f - T_\infty)}{D_S(C_w - C_\infty)}$ is the modified Dufour parameter, $Nc = \frac{\beta c (C_w - C_\infty)}{\beta_T (T_f - T_\infty)}$ is the regular double-diffusive buoyancy ratio, $Nr = \frac{(\rho_p - \rho_f)(N_w - N_\infty)}{\rho_f \beta_T (T_f - T_\infty)(1 - N_\infty)}$ is the nanofluid buoyancy

Table 4 The numerical of skin friction coefficient with $a = 0$ and $a = 0.5$

Bi	R	Pr	θ_w	Nd	Ln	Le	Ld	Nb	Nt	λ	M	Nc	Skin friction coefficient	
													$a = 0$	$a = 0.5$
0.2													1.43205	2.96707
0.4													1.36583	2.85068
0.6													1.32221	2.77284
	0												1.36251	2.85839
	0.5												1.34192	2.80810
	1												1.32089	2.75671
		3											1.32497	2.76526
		4											1.34192	2.80810
		5											1.35193	2.83360
			1										1.34876	2.82184
			1.4										1.33371	2.79157
			1.8										1.31274	2.74874
				0.1									1.26834	2.56823
				0.2									1.17796	2.29936
				0.3									1.07752	2.02579
					3								1.34801	2.81638
					4								1.34192	2.80810
					5								1.33795	2.80305
						5							1.34192	2.80810
						10							1.34160	2.80936
						15							1.33928	2.80541
							0.5						1.34192	2.80810
							1						1.34085	2.80503
							1.5						1.33978	2.80196
								0.2					1.36515	2.85138
								0.4					1.31797	2.76266
								0.6					1.26959	2.66933
									0.2				1.34910	2.82314
									0.4				1.33441	2.79227
									0.6				1.31846	2.75816
										0			1.58113	3.22750
										2			1.12634	2.44198
										4			0.73642	1.80525
											1		1.17104	2.47904
											2		1.49715	3.10837
											3		1.77371	3.64713
												1	1.09804	2.44336
												2	0.83753	2.06279
												3	0.58582	1.70306

Table 5 Numerical values of $-f''(0)$, $-\gamma'(0)$, $-\theta'(0)$ and $-\varphi'(0)$ for different physical parameters

Bi	R	Pr	θ_w	Nd	Ln	Le	Ld	Nb	Nt	a	λ	M	Nc	$-f''(0)$	$-\gamma'(0)$	$-\varphi'(0)$	$-\theta'(0)$
0.2														2.96707	1.50463	1.28818	0.26757
0.4														2.85068	1.50341	1.27248	0.41719
0.6														2.77284	1.50424	1.26552	0.50867
	0													2.85839	1.50345	1.27238	0.25574
	0.5													2.80810	1.50372	1.26835	0.46802
	1													2.75671	1.50957	1.27520	0.28380
		3												2.76526	1.50769	1.27218	0.45607
		4												2.80810	1.50372	1.26835	0.46802
		5												2.83360	1.50321	1.26976	0.47224
			1											2.82184	1.50071	1.26348	0.47644
			1.4											2.79157	1.50740	1.27434	0.45783
			1.8											2.74874	1.51675	1.28943	0.43212
				0.1										2.56823	1.57167	1.38537	0.30838
				0.2										2.29936	1.65304	1.52823	0.11343
				0.3										2.02579	1.74113	1.68545	−0.10123
					3									2.81638	1.49844	1.02955	0.47983
					4									2.80810	1.50372	1.26835	0.46802
					5									2.80305	1.50759	1.47537	0.45967
						5								2.80810	1.50372	1.26835	0.46802
						10								2.80936	2.26285	1.27719	0.45463
						15								2.80541	2.84139	1.28580	0.44357
							0.5							2.80810	1.50372	1.26835	0.46802
							1							2.80503	1.46854	1.26896	0.46828
							1.5							2.80196	1.43361	1.26957	0.46854
								0.2						2.85138	1.48668	1.18357	0.50788
								0.4						2.76266	1.52079	1.31270	0.42742
								0.6						2.66933	1.55364	1.35999	0.34719
									0.2					2.82314	1.49937	1.29030	0.47871
									0.4					2.79227	1.50818	1.25051	0.45699
									0.6					2.75816	1.51741	1.22730	0.43399
										1				3.99182	1.53308	1.30072	0.47469
										2				5.89049	1.57107	1.34290	0.48317
										3				7.43629	1.59502	1.36948	0.48839
											0			3.22750	1.46544	1.22729	0.45927
											2			2.44198	1.53371	1.29994	0.47455
											4			1.80525	1.58046	1.34835	0.48425
												1		2.47904	1.53351	1.30079	0.47471
												2		3.10837	1.47670	1.23908	0.46183
												3		3.64713	1.18758	1.18758	0.45060
													1	2.44336	1.52792	1.29302	0.47309
													2	2.06279	1.55163	1.31701	0.47793
													3	1.70306	1.57281	1.33831	0.48215

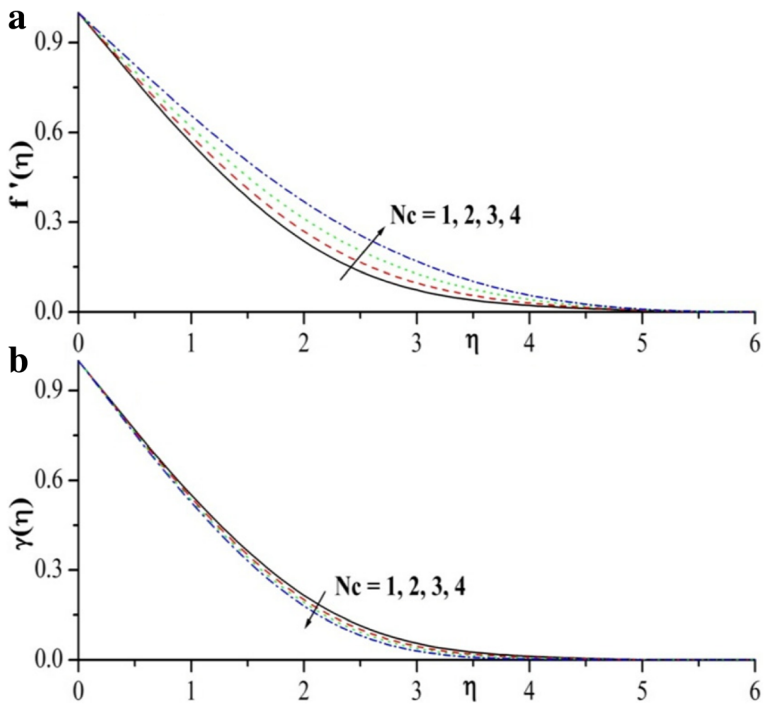

Fig. 2 a Velocity and **b** solute concentration profiles for variable values of Nc

ratio, $\lambda = \frac{(1-N_\infty)(\rho_f)g\beta_T(T_f-T_\infty)}{a\ u_w}$ is the mixed convection parameter, $R = \frac{16\sigma^* T_\infty^3}{3k^* k}$ is the radiation parameter, $Ld = \frac{D_{CT}(T_f-T_\infty)}{D_S(C_w-C_\infty)}$ Dufour Lewis number, $Ln = \frac{\nu}{D_B}$ is the nanofluid Lewis number, $Le = \frac{\nu}{D_s}$ is the regular Lewis number, $M = \frac{\sigma B_0^2}{\rho a}$ is the magnetic parameter, and $\Pr = \frac{\nu}{\alpha_m}$ is Prandtl number and $Bi = \frac{h_f}{k}\sqrt{\frac{\nu}{a}}$ is Biot number.

The physical quantities with practical interest in the study are skin friction coefficient, Nusselt number, regular Sherwood number, and nanoparticle Sherwood number.

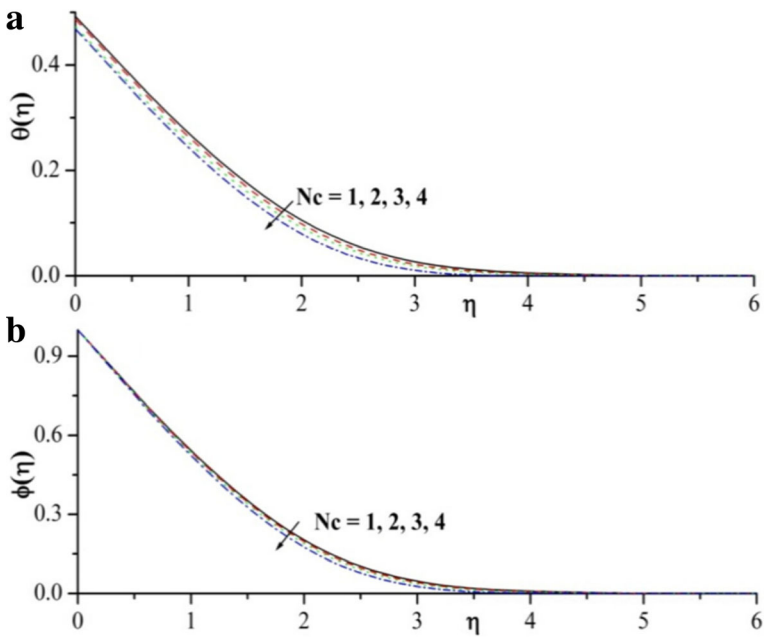

Fig. 3 a Temperature and **b** nanoparticle concentration profiles for variable values of Nc

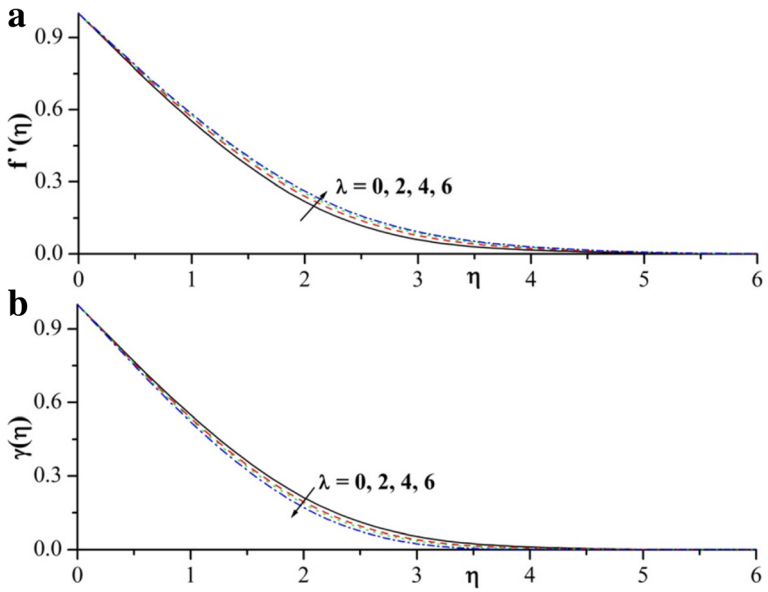

Fig. 4 **a** Velocity and **b** solute concentration profiles for variable values of λ

These parameters characterize surface drag, wall heat transfer, regular mass transfer, and nanoparticle mass transfer rates, respectively. These quantities are defined as

$$C_f = \frac{\tau_w}{\rho u_w^2/2}, Nu_x = \frac{xq_w}{k\left(T_f - T_\infty\right)}, Sh_x = \frac{xq_m}{D_S(C_w - C_\infty)}, Sh_{xn} = \frac{xq_{np}}{D_B(N_w - N_\infty)}, \tag{15}$$

where τ_w is the wall skin friction, q_w is the wall heat flux, and q_m and q_{np} are the solutal wall mass flux and nanoparticle wall mass flux at the surface of the sheet, respectively, which are given by the following expressions:

$$\tau_w = \mu\left(\frac{\partial u}{\partial y}\right)_{y=0} + \frac{\alpha}{\rho}\left(u\frac{\partial^2 u}{\partial x \partial y} v\frac{\partial^2 u}{\partial y^2} - 2\frac{\partial u}{\partial y}\frac{\partial v}{\partial y}\right)_{y=0}, q_w = -k\left(\frac{\partial T}{\partial y}\right) + q_{r_{y=0}},$$
$$q_m = -D_S\left(\frac{\partial C}{\partial y}\right)_{y=0} \text{ and } q_{np} = -D_B\left(\frac{\partial N}{\partial y}\right)_{y=0} \tag{16}$$

Following Kuznetsov and Nield (2010), the reduced local skin friction, local Nusselt number, reduced local

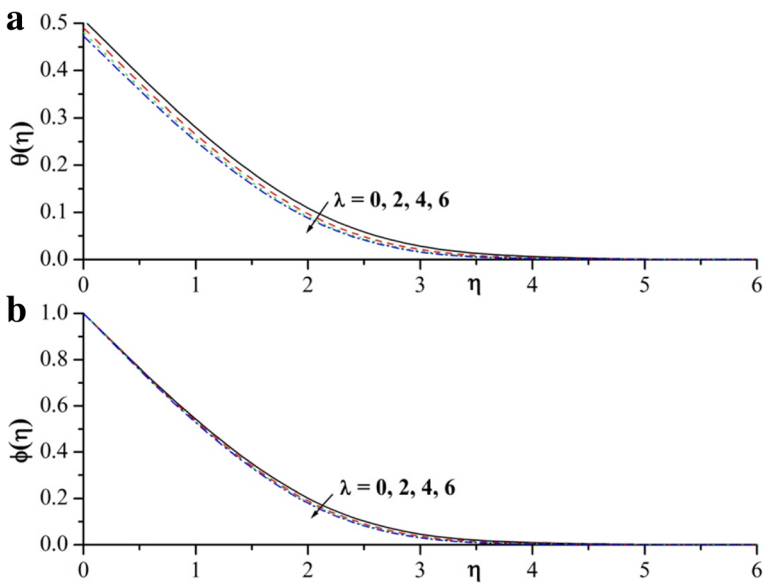

Fig. 5 **a** Temperature and **b** nanoparticle concentration profiles for variable values of λ

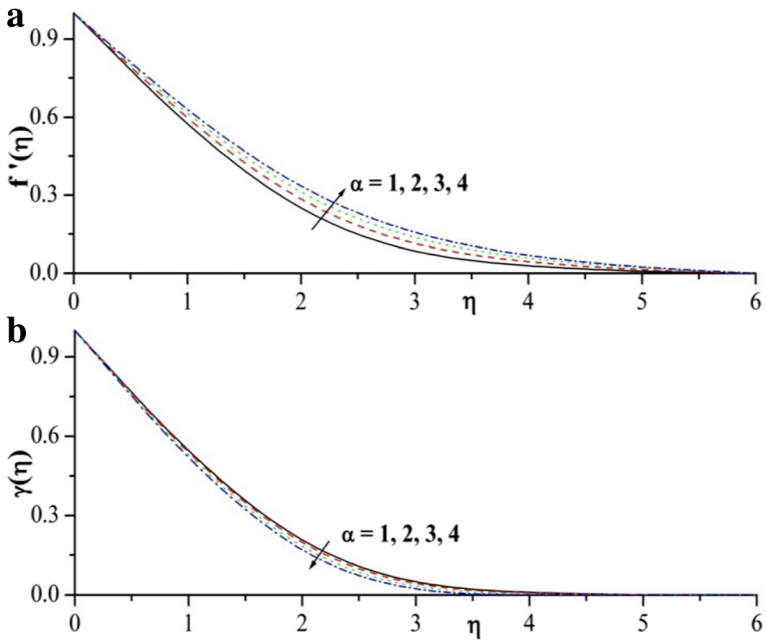

Fig. 6 a Velocity and **b** solute concentration profiles for variable values of *α*

Sherwood number, and reduced nanofluid Sherwood number can be introduced and represented as

$$C_f Re_x^{\frac{1}{2}} = (1+K)f''(0), Nu_x Re_x^{-\frac{1}{2}} = -\left(1+R\theta_w^3\right)\theta'(0),$$
$$Sh_x Re_x^{-\frac{1}{2}} = -\gamma'(0), \text{and } Sh_{xn} Re_x^{-\frac{1}{2}} = -\phi'(0), \tag{17}$$

where $Re_x = \frac{u_w(x)x}{\nu}$ is the local Reynolds number.

Methods

The reduced set of coupled similarity Eqs. (10)–(13) subject to boundary condition (14) are highly nonlinear in nature; thus, it is very difficult possess a closed form analytical solution. Therefore, it has been solved numerically by fourth–fifth order Runge–Kutta–Fehlberg integration scheme with the help of algebraic software Maple. The algorithm in Maple has been well tested for its accuracy and robustness. Thus, this has been used to solve a

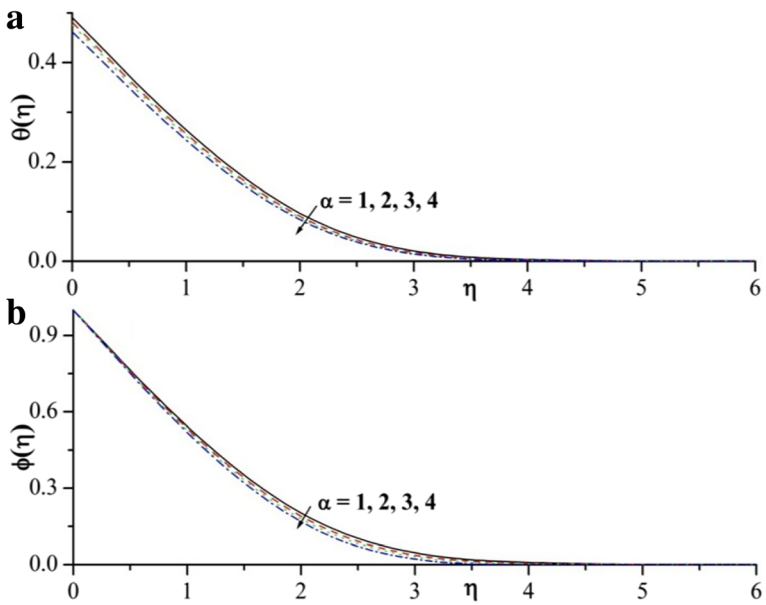

Fig. 7 a Temperature and **b** nanoparticle concentration profiles for variable values of *α*

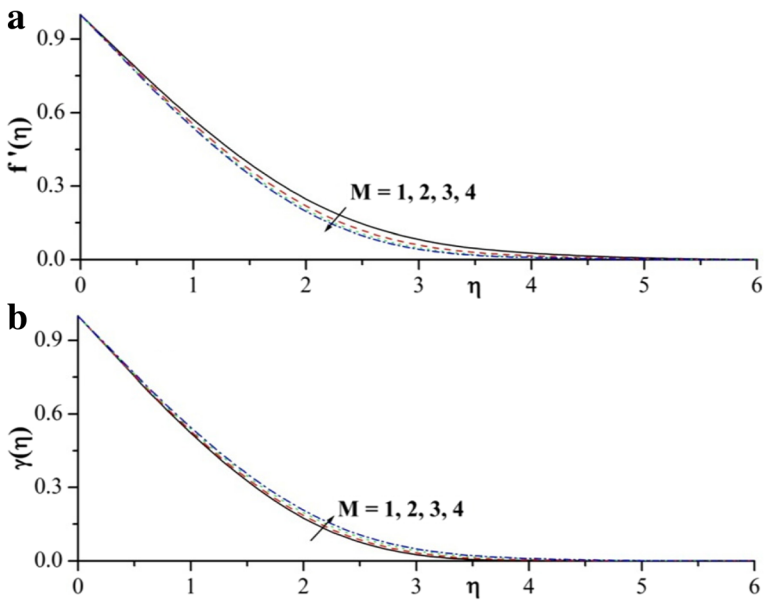

Fig. 8 a Velocity and **b** solute concentration profiles for variable values of *M*

wide range of nonlinear problems. In this method, we choose a finite value of $\eta \to \infty$ as η_6 in such a way that the boundary conditions are satisfied asymptotically. Table 1 depicts the validation of the current results by comparison with the existed literature for some special restricted cases (Khan and Pop (2010), Wang (1989), Gorla and Sidawi (1994). Further, the results are also compared with Khan and Pop (2010) and Goyal and Bhargava (2014) for numerous values of Nt and Nb which is tabulated in Tables 2 and 3. We notice that the comparison shows smart agreement for every value of Nt and Nb, which confirm that the current results are accurate. Numerical values of local Nusselt, Sherwood, and nanofluid Sherwood number are also depicted in Tables 4 and 5 for various

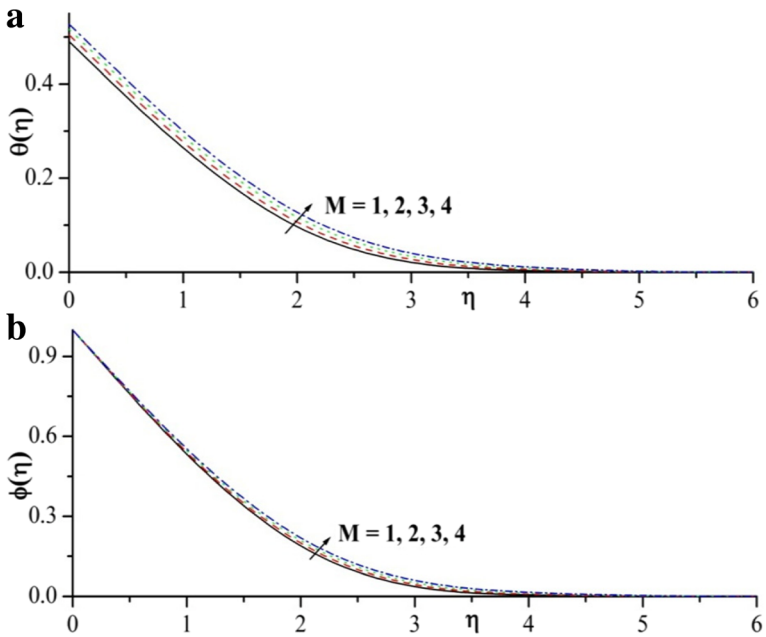

Fig. 9 a Temperature and **b** nanoparticle concentration profiles for variable values of *M*

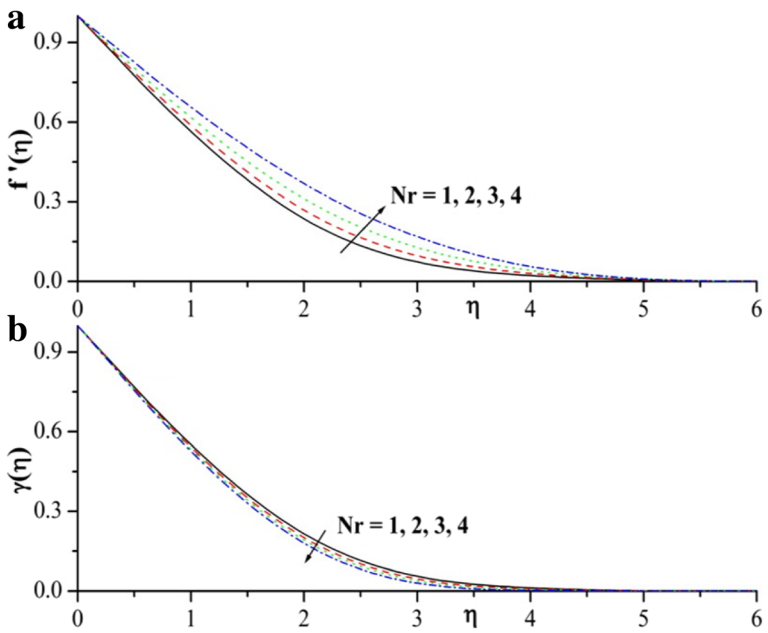

Fig. 10 **a** Velocity and **b** solute concentration profiles for variable values of Nr

concerned parameters. For numerical results, we considered the nondimensional parameter values as Bi = 0.5 , λ = 1 , α = 0.5 , Ld = 0.5 , Le = 5 , Ln = 4 , M = 1.5 , Nb = 0.3 , Nc = 0.1 , Nd = 0.01, Nt = 0.3 , Pr = 4 , R = 0.5, and θ_w = 1.2. These values are kept as common in the entire study except the variations in respective figures and tables.

Results and discussion

The main aim of this section is to analyze the effects of various physical parameters like Biot number, magnetic parameter, Prandtl number, radiation parameter, thermophoresis parameter, Brownian motion, and viscoelastic parameter. Hence, Figs. 2, 3, 4, 5, 6, 7, 8, 9, 10,

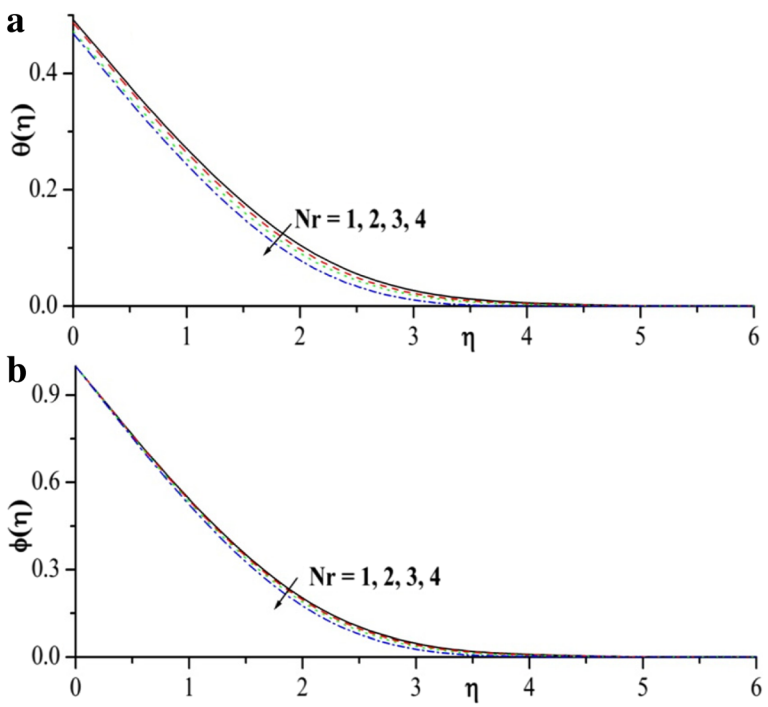

Fig. 11 **a** Temperature and **b** nanoparticle concentration profiles for variable values of Nr

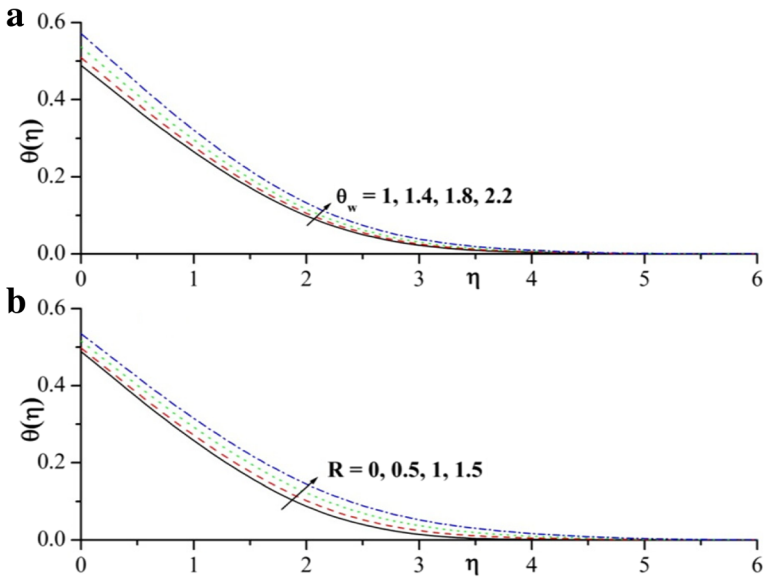

Fig. 12 **a**, **b** Temperature profiles for variable values of θ_w and R, respectively

11, 12, 13, 14, 15, 16, 17, and 18 have been plotted for such objective. Figure 2a describes the influences of double-diffusive buoyancy ratio parameter (Nc) on velocity and temperature profiles. It is observed that velocity profile is an increasing function of double-diffusive buoyancy ratio parameter; as a result, momentum boundary layer thickness increases. Figure 2b depicts that the solutal concentration reduced by increasing the buoyancy force parameter. Further, it is observed that the corresponding boundary layer is also reduced. Figure 3a, b is plotted to visualize the effects of double-diffusive buoyancy ratio parameter on temperature and nanoparticle concentration profile. From these figures, we observed that increasing values of the double-diffusive buoyancy ratio parameter lead to decrease the temperature, nanoparticle concentration, and corresponding boundary layer thickness as shown in Fig. 3a, b.

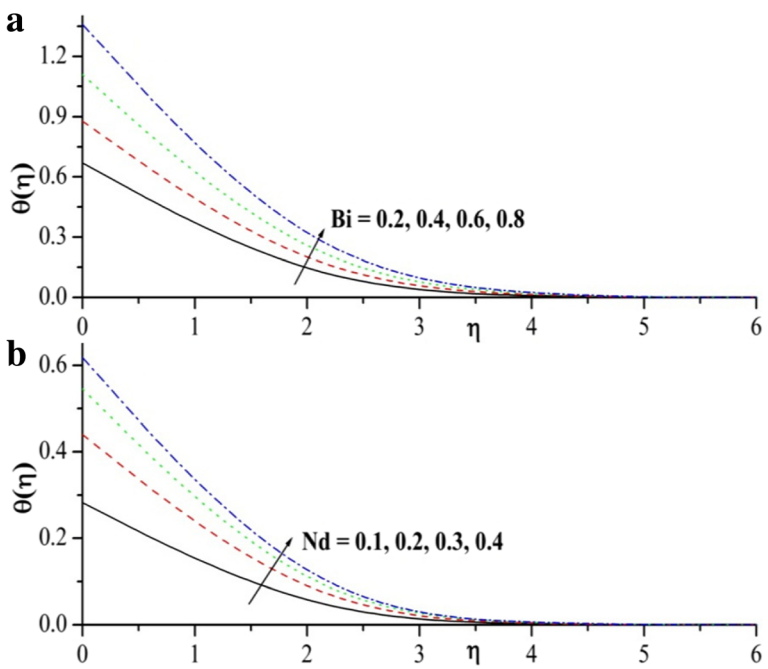

Fig. 13 **a**, **b** Temperature profiles for variable values of Bi and Nd, respectively

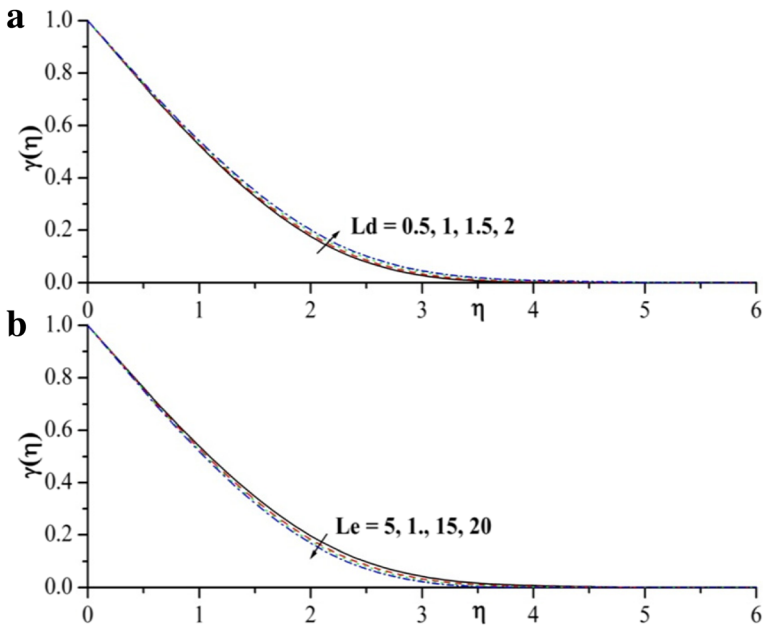

Fig. 14 a, **b** Solute concentration profiles for variable values of Ld and Le, respectively

Figure 4a, b shows the velocity and concentration profile for different values of mixed convection parameter (λ). It depicts that the velocity field and momentum boundary layer thickness increase by increasing mixed convection parameter as shown in Fig. 4a. Figure 4b illustrates that the solutal concentration profile and its boundary layer thickness are a decreasing function of mixed convection parameter. As viewed from Fig. 5a, b, the temperature and nanoparticle concentration profiles decreased significantly with an increase in mixed convection parameter.

Figures 6a, b and 7a, b show the velocity, solutal concentration, temperature, and nanoparticle concentration profile for different values of viscoelastic parameter (α), respectively. From this plot, it is evident that increasing values of viscoelastic parameter oppose the motion of

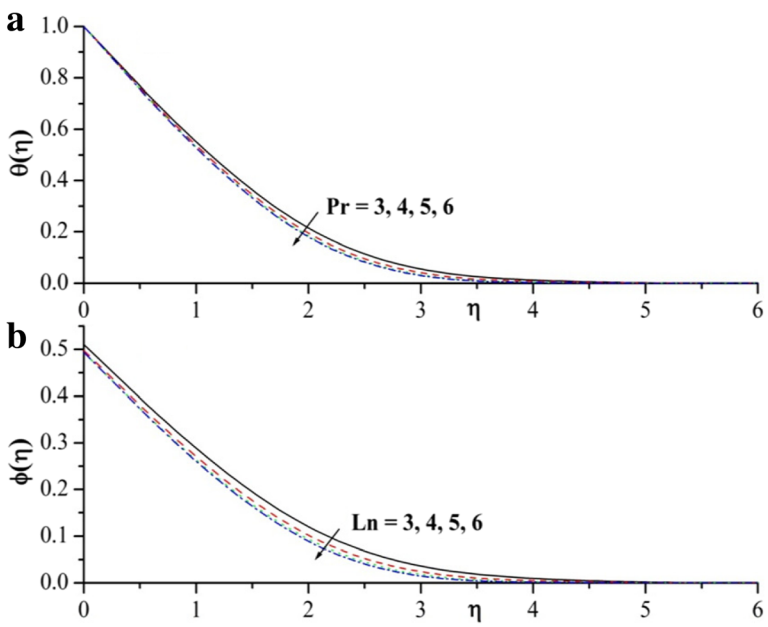

Fig. 15 a Temperature and **b** nanoparticle concentration profiles for variable values of Pr and Ln, respectively

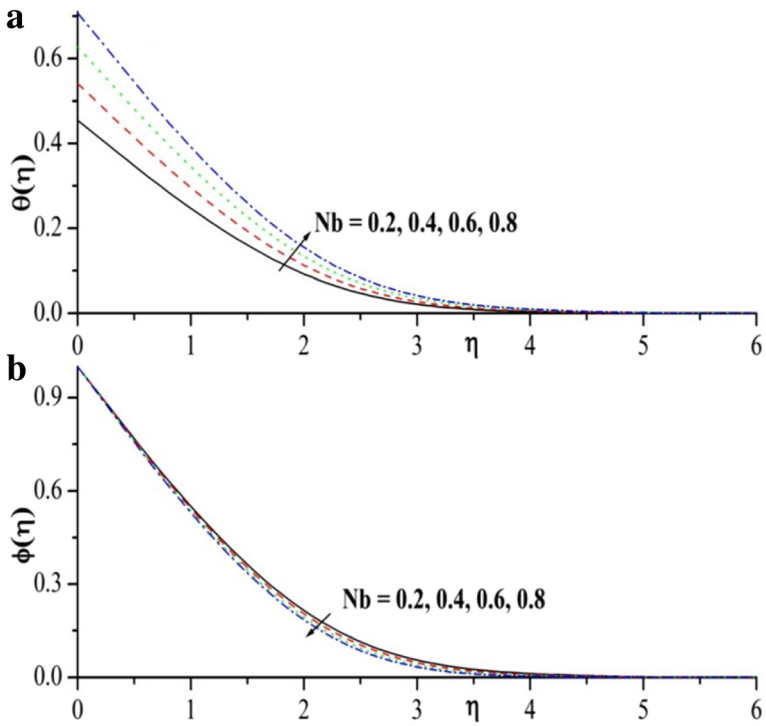

Fig. 16 a Temperature and **b** nanoparticle concentration profiles for variable values of Nb

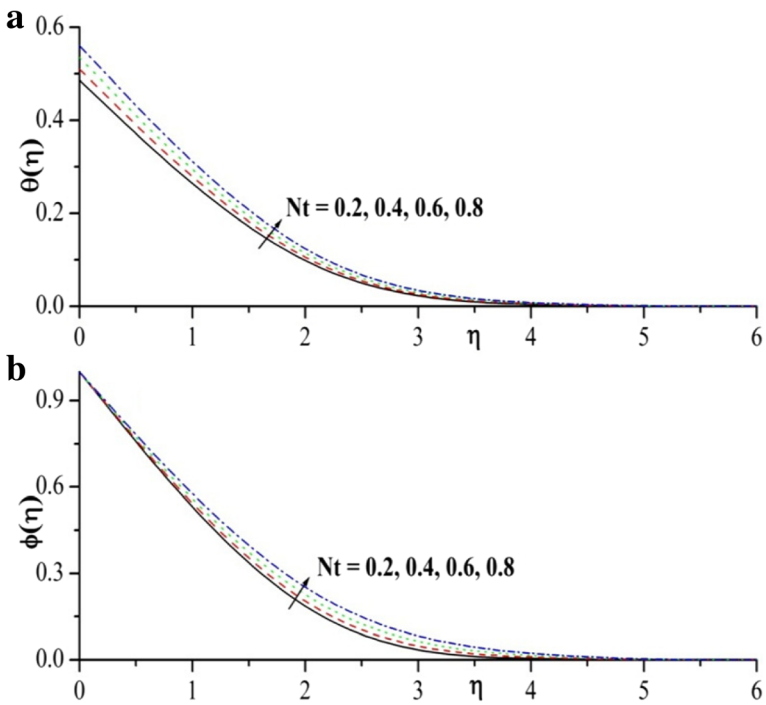

Fig. 17 a Temperature and **b** nanoparticle concentration profiles for variable values of Nt

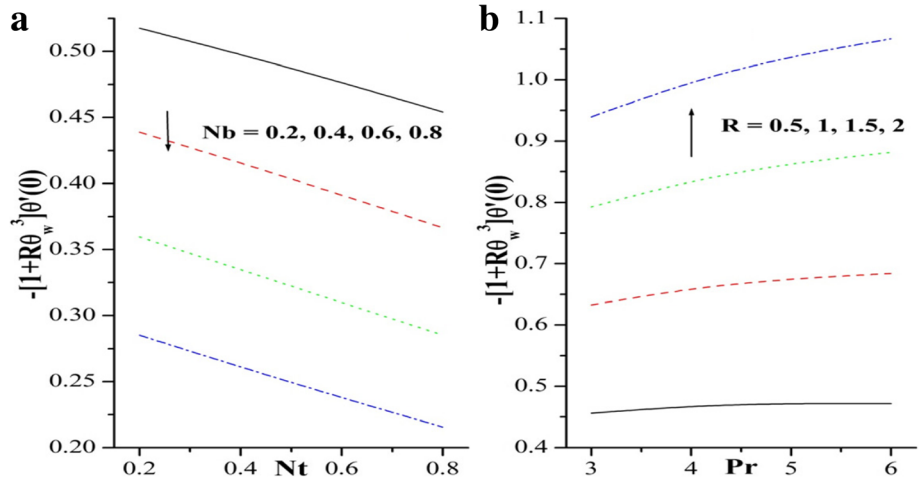

Fig. 18 a, **b** Influence of Nt and Pr with the various values of Nb and *R* on Nusselt number, respectively

the liquid close to the stretching sheet and assist the motion of the liquid faraway from the stretching sheet. Increasing values of viscoelastic parameter enables the liquid to flow at a faster rate, due to which there is decline in the heat transfer. This is responsible for the increase in momentum boundary layer, whereas the thermal, solute concentration, and nanoparticle concentration boundary layers reduce when the viscoelastic effects intensify.

Figure 8a, b, respectively, shows the effect of magnetic parameter (M) on the velocity and solute concentration profile. In general, the application of transverse magnetic field will result a restrictive type of force (Lorenz's force) similar to drag force which tends to resist the fluid flow and thus reducing its velocity. It is clear that, as the magnetic parameter increases, it reduced the velocity profile and enhanced the solute concentration profile. Figure 9a, b reveals the temperature and nanoparticle concentration profile for different values of magnetic parameter. It is observed from the above figures that, for increasing the values of M, the temperature and nanoparticle concentration distributions increase and also the corresponding boundary layer thickness.

The effect of nanofluid buoyancy ratio parameter (Nr) on velocity and solute concentration profile are depicted in Fig. 10a, b. It is evident from this figure that the velocity profile increases and solute concentration profile decreases for increasing the values Nr. The temperature and nanoparticle concentration profiles for different values of nanofluid buoyancy ratio parameter are presented in Fig. 11a, b, respectively. Thermal and nanoparticle boundary layer thickness decrease by increasing the nanofluid buoyancy ratio parameter.

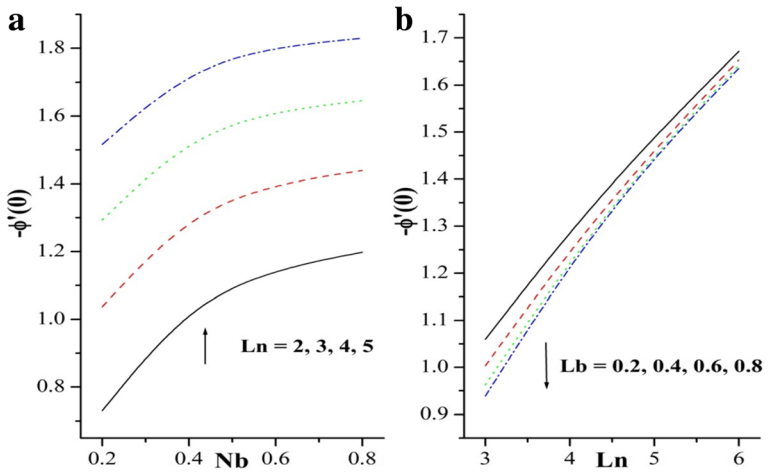

Fig. 19 a, **b** Influence of Nb and Ln with the various values of Ln and Ld on Sherwood number, respectively

Table 6 The numerical values of skin friction coefficient with different physical parameters with linear and nonlinear radiation

Bi	*R*	Pr	*a*	Nd	Ln	Le	Ld	Nb	Nt	*λ*	*M*	Nc	Nusselt number	
													Linear radiation	Nonlinear radiation
0.2													0.14372	0.26757
0.4													0.22566	0.41719
0.6													0.27708	0.50867
	0												0.25574	0.25574
	0.5												0.25407	0.46802
	1												0.24600	0.28380
		3											0.24744	0.45607
		4											0.25407	0.46802
		5											0.25664	0.47224
			1										0.27821	0.47469
			2										0.28283	0.48317
			3										0.28565	0.48839
				0.1									0.16878	0.30838
				0.2									0.05850	0.11343
				0.3									−0.07540	−0.10123
					3								0.26013	0.47983
					4								0.25407	0.46802
					5								0.24975	0.45967
						5							0.25407	0.46802
						10							0.24709	0.45463
						15							0.24131	0.44357
							0.5						0.25407	0.46802
							1						0.25425	0.46828
							1.5						0.25443	0.46854
								0.2					0.27452	0.50788
								0.4					0.23288	0.42742
								0.6					0.18971	0.34719
									0.2				0.27936	0.47871
									0.4				0.26948	0.45699
									0.6				0.25883	0.43399
										0			0.27034	0.45927
										2			0.27770	0.47455
										4			0.28247	0.48425
											1		0.27811	0.47471
											2		0.27120	0.46183
											3		0.26518	0.45060
												1	0.27720	0.47309
												2	0.27975	0.47793
												3	0.28196	0.48215

Figure 12a, b demonstrates the effect of temperature ratio and radiation parameter on temperature profile, respectively. Here, we observed that the temperature profile is an increasing function of temperature ratio and radiation parameter; as a result, thermal boundary layer thickness also increases. This is due to the fact that enhancement in the radiation parameter implies a decrease in the Rosseland radiation absorptive. Hence, the

divergence of radiative heat flux q_r increases as absorption coefficient decreases. Therefore, the rate of radiative heat transferred to the fluid increases and consequently the fluid temperature and simultaneously the velocity of the fluid also increases.

Figure 13a, b describes the influences of Biot number and modified Dufour parameter on temperature profiles, respectively. The influence of Biot number (Bi) on the temperature profile is shown in Fig. 13a. The stronger convection leads to the maximum surface temperatures which appreciably enhance the temperature and the thermal boundary layer thickness. From Fig. 13b, it is noticed that the thermal boundary layer thickness increases by increasing the modified Dufour parameter (Nd). The variation of dimensionless solute concentration with Dufour Lewis number and regular Lewis number is illustrated Fig. 14a, b. An increase Dufour Lewis number enhances the solute concentration in the boundary layer thickness. But in case of regular Lewis number, it reduces the solute concentration in the boundary layer thickness as shown in Fig. 14b.

The effect of Prandtl number and nanofluid Lewis number on temperature and nanoparticle concentration profiles are exhibited in Fig. 15a, b, respectively. From Fig. 15a, we observed that an increase in the Prandtl number is seen to decrease the fluid temperature above the sheet. Physically it means that, the thermal boundary layer becomes thinner for the larger Prandtl number. The Prandtl number signifies the ratio of momentum diffusivity to thermal diffusivity. Hence, the Prandtl number can be used to increase the rate of cooling in conducting flows. From another plot, it is evident that increasing values of Lewis number reduces nanoparticle concentration profile; physically, it means that Lewis number lessens the mass diffusivity which in turn lessens the penetration depth of the concentration boundary layer as shown in Fig. 15b.

Figure 16a, b portraits the consequences of Brownian motion parameter on temperature and nanoparticle concentration profile. The Brownian motion parameter (Nb) will increase the random motion of the fluid particles and boundary layer thickness conjointly, which ends up in an additional heat to provide. Therefore, temperature profile will increase. However, nanoparticle concentration profiles show an opposite behavior because increasing Brownian motion parameter enhances the nanoparticle volume fraction transfer rate. This can be shown in Fig. 16b. It is interesting that the variation of the Brownian motion parameter does not show a significant influence on the concentration and temperature profiles, but its effect on the velocity profiles is obvious in the vicinity of the wall.

The development of the thermophoresis parameter (Nt) on temperature and nanoparticle concentration profiles is inspecting in Fig. 17a, b. Raising the values of thermophoresis parameter enhance both temperature $\theta(\eta)$ and concentration $\phi(\eta)$ profiles. Physically, thermophoretic parameter increases the density of the thermal boundary layer. As a result, temperature rises with the improvement in thermophoresis. Further, the boundary layer thickness is higher for larger values of thermophoresis parameter. It is a mechanism which little particle area unit force off from the new surface to a chilly one. As a result, it maximizes the temperature and nanoparticle concentration of the fluid. The combined effects of Brownian motion and thermophoresis parameters on the reduced Sherwood number are shown in Fig. 18a. An increase in the values of Brownian motion and thermophoresis parameters results a decrease in Sherwood number, but Sherwood number increases by increasing values of the radiation parameter and Prandtl number. This can be shown in Figs. 18b and 19a, b.

Conclusions

The present work analyzes the double diffusion boundary layer flow of a viscoelastic nanofluid over a stretching sheet including the nonlinear thermal radiation, mixed convection, and magnetic effects. The radiative heat flux term in the energy equality is presented by means of the nonlinear Rosseland diffusion approximation. It should also be concluded that in contrast to the linear Rosseland diffusion approximation, when use is made of the nonlinear one, the problem is also governed by the newly temperature ratio parameter θ_w. The results presented indicate quite clearly that θ_w, which is an indicator of the small/large temperature difference between the surface and the ambient fluid, has a relevant effect on heat transfer characteristics and temperature distributions within the flow region generated by an isothermal sheet stretched. Also, the effects of various standards of emerging parameters are discussed for velocity, temperature, nanoparticle concentration, and solute concentration. The key results of the present analysis can be listed as below.

- Magnetic field reduces the velocity the profile and enhances the temperature, solute, and nanoparticle concentration profiles.
- An increasing value of the regular buoyancy ratio, nanofluid buoyancy ratio, viscoelastic parameter, and mixed convection parameter is to increase the momentum boundary layer thickness and to decrease the thermal, solutal, and nanoparticle boundary layer thickness.
- Brownian motion parameter that has an opposite effect on temperature and nanoparticle concentration profiles but similar effect on temperature and nanoparticle concentration profiles is observed in case of thermophoresis parameter.

- Increasing values of temperature ratio parameter θ_w extinguishes the rate of heat transfer $|\theta'(0)|$ for fixed Pr and R.
- The temperature ratio parameter θ_w and the thermal radiation parameter R have the same effect. From a qualitative point of view, temperature increases within creasing θ_w and R. However, thermal boundary layer thickness decreases when the Prandtl number increases.
- In coolant factor, nonlinear thermal radiation is a superior copier to linear thermal radiation (Table 6).
- The temperature profile as well as thermal boundary layer thickness increases with an increase in both Biot and modified Dufour parameter.
- Solutal concentration profile increases for higher values of Dufour Lewis number whereas it decreases with increase in values of regular Lewis number.

Authors' contributions

GK has involved in conception and design of the problem. NGR has involved in analysis and interpretation of data. MS has involved in drafting the manuscript or revising it critically for important intellectual content. BJG has given final approval of the version to be published. All authors read and approved the final manuscript.

Competing interests

The authors declare that they have no competing interests.

Publisher's Note

Author details

[1]Department of Studies and Research in Mathematics, Kuvempu University Shankaraghatta, Shimoga, Karnataka 577 451, India. [2]Faculty of Engineering, Department of Engineering Mathematics, Christ University, Mysore Road, Bengaluru 560074, India.

Received: 20 May 2017 Accepted: 12 July 2017
Published online: 18 August 2017

References

Beg, O. A., Uddin, M. J., Rashidi, M. M., & Kavyani, N. (2014). Double-diffusive radiative magnetic mixed convective slip flow with Biot and Richardson number effects. *Journal of Engineering Thermophysics, 23*(2), 79–97.

Buongiorno, J. (2006). Convective transport in nanofluids. *ASME Journal Heat Transfer, 128*, 240–250.

Choi, S. U. S. (1995). Enhancing thermal conductivity of fluids with nanoparticles. *Proceedingsof the 1995 ASME International Mechanical Engineering Congress and Exposition, San Francisco, USA ASME FED 231/MD, 66*, 99–105.

Crane, L. J. (1970). Flow past a stretching plate. *ZAMP, 21*, 645–655.

Eastman, J. A., Choi, S. U. S., Li, S., Yu, W., & Thompson, L. J. (2001). Anomalously increased effective thermal conductivity of ethylene glycol-based nanofluids containing copper nanoparticles. *Applied Physics Letters, 78*, 718–720.

Gaikwad, S. N., Malashetty, M. S., & Rama Prasad, K. (2007). An analytical study of linear and non-linear double diffusive convection with Soret and Dufour effects in couple stress fluid. *International Journal of Non-Linear Mechanics, 42*, 903–913.

Ganesh Kumar, K., Rudraswamy, N. G., Gireesha, B. J., & Krishnamurthy, M. R. (2017). Influence of nonlinear thermal radiation and viscous dissipation on three-dimensional flow of Jeffrey nano fluid over a stretching sheet in the presence of joule heating. *Nonlinear Engineering*, https://doi.org/10.1515/nleng-2017-0014.

Gorla, R. S. R., & Sidawi, I. (1994). Free convection on a vertical stretching surface with suction and blowing. *Applied Scientific Research, 52*, 247–257.

Goyal, M., & Bhargava, R. (2014). Finite element solution of double-diffusive boundary layer flow of viscoelastic nanofluids over a stretching sheet. *Computational Mathematics and Mathematical Physics, 54*(5), 848–863.

Haq, R. U., Nadeem, S., Khan, Z. H., & Okedayo, T. G. (2014). Convective heat transfer and MHD effects on Casson nanofluid flow over a shrinking sheet. *Central European Journal of Physics, 12*(12), 862–871.

Hayat, T., Farooq, M., & Alsaedi, A. (2014). Melting heat transfer in the stagnation-point flow of Maxwell fluid with double-diffusive convection. *International Journal of Numerical Methods for Heat & Fluid Flow, 24*(3), 760–774.

Hsiao, K. L. (2017b). Micropolar nanofluid flow with MHD and viscous dissipation effects towards a stretching sheet with multimedia feature. *International Journal of Heat and Mass Transfer, 112*, 983–990.

Hsiao, K.-L. (2014). Nanofluid flow with multimedia physical features for conjugate mixed convection and radiation. *Computers & Fluids, 104*(20), 1–8.

Hsiao, K.-L. (2016). Stagnation electrical MHD nanofluid mixed convection with slip boundary on a stretching sheet. *Applied Thermal Engineering, 98*(5), 850–861.

Hsiao, K.-L. (2017a). To promote radiation electrical MHD activation energy thermal extrusion manufacturing system efficiency by using Carreau-Nanofluid with parameters control method. *Energy, 130*(1), 486–499.

Hsiao, K.-L. (2017b). Combined electrical MHD heat transfer thermal extrusion system using Maxwell fluid with radiative and viscous dissipation effects. *Applied Thermal Engineering, 112*, 1281–1288. doi:10.1016/j.applthermaleng.2016.08.208.

Kang, H. U., Klm, S. H., & OhE, J. M. (2006). Particles of thermal conductivity of nanofluid using experimental effect i n particle volume. *Experimental Heat Transfer, 19*(3), 181–191.

Khan, W. A., & Aziz, A. (2011). Double-diffusive natural convective boundary layer flow in porous medium saturated with a nanofluid over a vertical plate: prescribed surface heat, solute and nanoparticle fluxes. *International Journal of Thermal Sciences, 726*, 2154–2160.

Khan, W. A., & Gorla, R. S. R. (2011). Heat and mass transfer in non-Newtonian nanofluids over a non-isothermal stretching wall. *Proceedings of the Institution of Mechanical Engineers, Part N: Journal of Nanoengineering and Nanosystems, 225*(4), 155–163.

Khan, W. A., & Pop, I. (2010). Boundary layer flow of a nanofluid past a stretching sheet. *International Journal of Heat and Mass Transfer, 53*, 2477–2483.

Kuznetsov, A. V., & Nield, D. A. (2010). Natural convective boundary-layer flow of a nanofluid past a vertical plate. *International Journal of Thermal Sciences, 49*, 243–247.

Nadeema, S., Haq, R. U., & Khan, Z. H. (2014). Numerical study of MHD boundary layer flow of a Maxwell fluid past a stretching sheet in the presence of nanoparticles. *Journal of the Taiwan Institute of Chemical Engineers, 45*(1), 121–112.

Nield, D. A., & Kuznetsov, A. V. (2011). The Cheng–Minkowycz problem for the double-diffusive natural convective boundary layer flow in a porous medium saturated by a nanofluid. *International Journal of Heat and Mass Transfer, 54*, 374–378.

Rudraswamy, N. G., Gireesha, B. J., & Chamkha, A. J. (2015). Effects of magnetic field and chemical reaction on stagnation-point flow and heat transfer of a nanofluid over an inclined stretching sheet. *Journal of Nanofluids, 4*(2), 239–246.

Rudraswamy, N. G., Ganesh Kumar, K., Gireesha, B. J., & Gorla, R. S. R. (2016). Soret and Dufour effects in three-dimensional flow of Jeffery nanofluid in the presence of nonlinear thermal radiation. *Journal of Nanoengineering and Nanomanufacturing, 6*(4), 278–287.

Rudraswamy, N. G., Ganesh Kumar, K., Gireesha, B. J., & Gorla, R. S. R. (2017). Combined effect of Joule heating and viscous dissipation on MHD three dimensional flow of a Jeffrey nanofluid. *Journal of Nanofluids, 6*(2), 300–310.

Rudyak, V. Y., Belkin, A. A., & Tomilina, E. A. (2010). On the thermal conductivity of nnanofluids. *Technical Physics Letters, 36*(7), 660–662.

Sakiadis, B. C. (1961a). Boundary-layer behavior on continuous solid surfaces: I. Boundary-layer equations for two-dimensional and axisymmetric flows. *AIChE, 7*, 26–28.

Sakiadis, B. C. (1961b). Boundary-layer behavior on continuous solid surfaces: II. The boundary layer on a continuous flat surface. *AIChE, 7*, 221–225.

Sharma, A. K., Dubey, G. K., & Varshney, N. K. (2012). Effect of kuvshinski fluid on double-diffusive convection-radiation interaction on unsteady MHD flow over a vertical moving porous plate with heat generation and soret effects. *Advances in Applied Science Research, 3*(3), 1784–1794.

Shehzad, S. A., Hayat, T., & Alsaedi, A. (2015). MHD flow of Jeffrey nanofluid with convective boundary conditions. *Journal of the Brazilian Society of Mechanical Sciences and Engineering, 37*, 873–883.

Wang, C. Y. (1989). Free convection on a vertical stretching surface. *ZAMM-Journal of Applied Mathematics and Mechanics/Zeitschrift für Angewandte Mathematik und Mechanik, 69*, 418–420.

Wang, X., Xu, X., & Choi, S. U. S. (1999). Thermal conductivity of nanoparticle fluid mixture. *Journal of Thermophysics and Heat Transfer, 13*, 474–480.